COBEM 2023 27TH INTERNATIONAL CONGRESS OF MECHANICAL ENGENEERING

ABCM Brazilian Society of Mechanical Sciences and Engineering
27th ABCM International Congress of Mechanical Engineering
December 04-08, 2023, Florianópolis-SC, Brazil

COB-2023-0926
DISPLACEMENT FLOWS OF MISCIBLE FLUIDS THROUGH AXISYMMETRIC EXPANSION-CONTRACTIONS

Frederico Resende de Carvalho
Rafael Menezes de Oliveira
Department of Mechanical Engineering, PUC-RJ : Pontifícia Universidade Católica do Rio de Janeiro, Rua Marquês de São Vicente 225, Rio de Janeiro, RJ 22453-900, Brazil
frerecar@aluno.puc-rio.br
rmo@puc-rio.br

Abstract. *One critical step during an oil well construction is the primary cementing process. Simply classified as "the process of placing cement in the annulus between the casing and the formation exposed to the wellbore", although it has a simple definition, cementing operation is an important phase of well construction that provides zonal isolation, protects the casing from corrosion, and adds mechanical stability to the well. In this process, during the drilling stage, cross-sectional irregularities may appear on the open hole section due to poorly consolidated formation rocks. Such irregularities can be described as washouts. As a result, the placement of cement slurry occurs through a displacement process in an irregular annular space. Motivated by this industrial process, the current work employs Direct Numerical Simulation to investigate the displacement process between two miscible Newtonian fluids in an annular space containing an abrupt expansion followed by a contraction on the external radius. The axisymmetric Navier-Stokes equations in cylindrical coordinates are solved coupled with a convection-diffusion equation for a scalar that measures the concentration of the displaced fluid. To investigate the influence of miscibility, we consider neutrally buoyant flows for a constant injected flow rate with fixed values of the viscosity ratio and fixed size of the rectangular washout to investigate the influence of different values of the Péclet number. Our results calculate displacement efficiency values close to 100%. These high values motivate further investigations of miscibility to improve displacement efficiency in the industrial setting.*

Keywords: *Miscible, Displacement, Newtonian, Fluid, Péclet.*

1. INTRODUCTION

In the oil and gas industry, a primary cementing operation was defined by Nelson (1990) as: *"The process of placing cement in the annulus between the casing and the formation exposed to the wellbore"* . Its importance is intrinsically associated with the immense complexity of the physical and chemical phenomena that occur during all stages, being one of the most critical stages during the construction process of injection or producer wells.

Such criticality is primarily related to crucial issues related to well safety and consequently to the mitigation of risks associated with exposure of the environment to hydrocarbons and other toxic fluids. Therefore, the process of cementing oil wells is an important function amid the set of safety barrier systems, being one of the key elements for the integrity of the well.

The fundamental care and basic objective of this type of process aims the hydraulic isolation and the permanent mechanical stability between the casing and the walls of the open hole, in such a way that there is no undesirable migration of fluids towards the interior of the annular space, between the open hole or productive zones of interest and the casing. As well as interrupting the motion of fluids from the well to the formation, avoiding risks of fracturing the rock formation, and as a consequence, protecting the casing against corrosion caused by harmful fluids arising from the rock formation and providing, duly to the well environment, the necessary hydraulic and mechanic stability for the casing string throughout its productive life.

Some recent scientific works have studied the hydrodynamic behavior of the displacement of the drilling fluid by a cementing system. Amid them, we highlight the studies carried out by Naccache *et al.* (2018), presenting a numerical study about the displacement of two fluids through a vertical duct containing an abrupt expansion in the cross section. The resolution of the mass and momentum conservation equations for this two-phase axisymmetric flow problem was approached using finite volume methods. Several flow patterns along the irregularity and displacement efficiency for different pairs of fluids were discussed: (case 1) visco-plastic fluid displacing a newtonian fluid, (case 2) newtonian fluid displacing a visco-plastic fluid and (case 3) a visco-plastic fluid displacing a second visco-plastic fluid. The authors

observed that inertial effects (larger number of Reynolds) tend to displace the interface between the fluids towards the contraction wall of the irregular section, resulting in lower displacement efficiencies.

Etrati *et al.* (2020) study the effects of the length of the washouts, pumping rates, densities and viscosity ratios during the displacement of the drilling fluid by a spacer system representing the cementing process of a vertical well, through the analysis of the results of $3D$ simulations. The authors used 6 pairs of fluids in the Newton-Bingham displacement and analyzed the effects of displacement with fluids of different densities, viscosity ratios, and as a function of different pumping rates. The results show that increasing the pumping rate yields different effects on the two-phase displacement. As the Reynolds number is increased, the interface is shifted towards the output of the washout. In simulations with a sufficiently high Reynolds number, the flow destabilizes within the washout, concluding that, such processes may or may not improve the displacement process.

Renteria *et al.* (2018) described the effects of irregularities during displacement flow during a primary cementing operation of highly deviated wells. The studies investigate the effects of washouts during drilling fluid removal through experimental analyzes and two-dimensional computer simulations. The authors found that increasing the washout diameter reduces the displacement efficiency, for both configurations between open hole and casing (concentric and eccentric). Increasing the washout length is less clear, pointing to a possible improvement in efficiency. For all cases, the potential risk of contamination of the cementing system in the washout area is evident.

Zare *et al.* (2017) pointed out the effects of buoyancy on the formation of micro annuli in the annulus wall through the displacement of a Bingham fluid by a Newtonian fluid, employing different viscosities, and different Bingham, Froude, and Reynolds numbers. The $2D$ model mixes finite elements and finite volumes with the inclusion of buoyancy terms. The results obtained demonstrate that, by increasing the viscosity ratio, the formation of micro annuli on the walls of the annulus increases. By increasing the parameters related to buoyancy, the formation of micro annuli is reduced, therefore increasing the displacement efficiency. Increasing the parameter corresponding to the ratio between the displaced fluid yield stress and the viscous tension of the displacing fluid, classified as Newton-Bingham number, decreases the formation of micro annuli. For high buoyancy values, the residual layer is also reduced.

Roustaei *et al.* (2015a) carried out computational studies on the flow of a Bingham fluid along a narrow flat channel, containing an expanded irregularity, considering non-inertial flows. They analyzed different types of washouts geometries and the formation of areas with static fluid. The authors showed that, in the case of relatively deep washouts, with fluids with high yield stresses, the fluid behaves in such a way as to "self-select" the flow region in such a manner that is independent of the geometry washout. In the second part of this work, Roustaei *et al.* (2015b) extend the previous analysis to stationary laminar inertial flows and investigated the effects of the Bingham and Reynolds numbers $(10 \leq Re \leq 500)$. Increasing the Reynolds number results in increasing regions with static fluid. The authors conclude that these results are important for the industry, since the usual perception, although not always true, is that: the conditioning efficiency will benefit by increasing the flow regime.

These and other works such as Bittleston *et al.* (2022); Savery *et al.* (2007) have not considered the influence of miscibility in the displacement of fluids in annular spaces. The current work begins to analyze the relevance of this parameter by considering a simplified scenario in which the fluids are Newtonian and have the same density. The high-efficiency values obtained motivate further investigations.

2. MODELLING

Our study focuses on a configuration that considers the displacement between two miscible Newtonian fluids through an irregular, rectangular washout in an annular space which may be considered as the annulus between the casing and the open hole. The two-phase flow solves axisymmetric Navier-Stokes equations in cylindrical coordinates and consider the fluids to be miscible and incompressible. At time $t = 0$, $Fluid\ 1$ (blue fluid in Fig. 1) is injected at a constant flow rate with a developed velocity profile. The remaining annular space, as well as the irregularity, is filled up with $Fluid\ 2$ (yellow fluid in Fig. 1).

Here, R_{int} represents the inner radius of the annulus of the well, that is the outer radius of the concentric casing. In addition, the external radius R_{ext} corresponds to the open hole of the well, and contains an irregularity in the cross-section or abrupt expansion (washout), with length L and depth H. $Fluid\ 1$ represents the displacing fluid with viscosity μ_1, while $Fluid\ 2$ is the fluid to be displaced fluid with μ_2.

We solve the Navier-Stokes equations with variable viscosity, the conservation of mass, and an advection-diffusion equation for a scalar field that represents the concentration of the displaced fluid. In dimensioless variables, these equations are given by:

$$\frac{\partial v_r}{\partial t} + v_r\frac{\partial v_r}{\partial r} + v_z\frac{\partial v_r}{\partial z} = \frac{1}{R_e}\left\{\frac{\partial}{\partial r}\left[2\mu\frac{\partial v_r}{\partial r}\right] + \frac{\partial}{\partial z}\left[\mu\left(\frac{\partial v_r}{\partial z} + \frac{\partial v_z}{\partial r}\right)\right] + 2\mu\left(\frac{1}{r}\frac{\partial v_r}{\partial r} - \frac{v_r}{r^2}\right) - \frac{\partial p}{\partial r}\right\}, \tag{1}$$

$$\frac{\partial v_z}{\partial t} + v_r\frac{\partial v_z}{\partial r} + v_z\frac{\partial v_z}{\partial z} = \frac{1}{R_e}\left\{\frac{\partial}{\partial z}\left[2\mu\frac{\partial v_z}{\partial z}\right] + \frac{\partial}{\partial r}\left[\mu\left(\frac{\partial v_z}{\partial r} + \frac{\partial v_r}{\partial z}\right)\right] + \frac{\mu}{r}\left(\frac{\partial v_z}{\partial r} + \frac{\partial v_r}{\partial z}\right) - \frac{\partial p}{\partial z} + Fc\right\}, \tag{2}$$

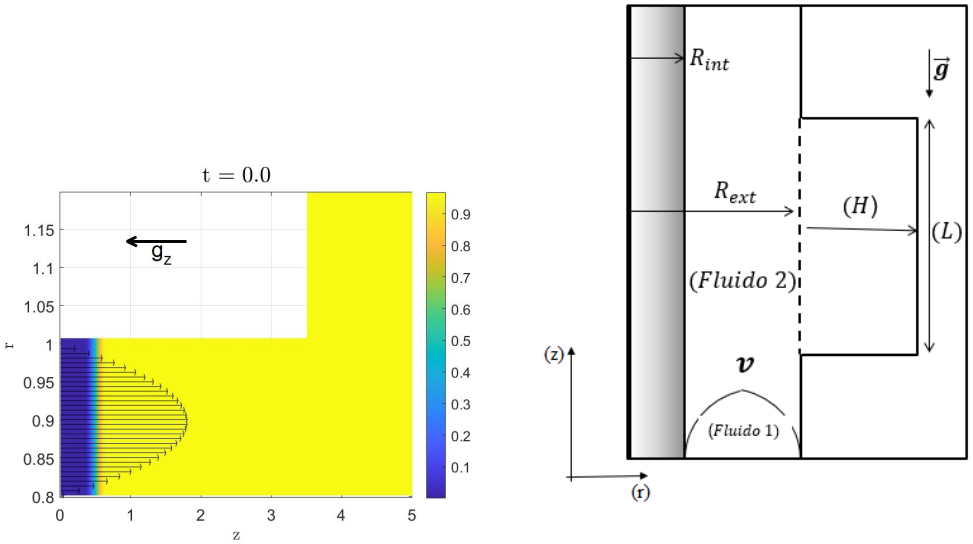

Figure 1. Figure illustrating the initial conditions and rectangular washout of the geometry.

$$\frac{1}{r}\frac{\partial(rv_r)}{\partial r} + \frac{\partial v_z}{\partial z} = 0, \tag{3}$$

$$\frac{\partial c}{\partial t} + v_r\frac{\partial c}{\partial r} + v_z\frac{\partial c}{\partial z} = \frac{1}{P_e}\left[\frac{1}{r}\frac{\partial}{\partial r}\left(r\frac{\partial c}{\partial r}\right) + \frac{\partial^2 c}{\partial z^2}\right]. \tag{4}$$

The equations were made dimensionless by considering R_{ext} as the characteristic length of the problem, and U as the characteristic velocity that represents the average inflow velocity of the injected $Fluid\ 1$. The characteristic pressure is $\mu_1\frac{U}{R_{ext}}$. v_r and v_z represent the velocity components along the radial and axial axes, respectively. r corresponds to the radial coordinate, z corresponds to the longitudinal coordinate along the axial domain, t is time, p is the pressure, and μ is a viscosity function that captures the dynamic viscosities of each fluid and depends upon the concentration of the displaced fluid.

We use a single-fluid model, where a single Navier-Stokes equation is solved to describe the dynamics of both fluids with their properties varying in space. It is at the interface between the fluids that these properties vary abruptly. In this approach for miscible and incompressible fluids, the viscosity function is variable and correlated with the concentration scalar field c, which measures the concentration of the resident fluid. When this fluid is pure, it has a concentration of $c = 1$. The domain inlet is defined by injecting $Fluid\ 1$ with a concentration of $c = 0$. Any intermediate value between $0 < c < 1$ can be used to access the diffuse interface between the fluids. In other words, the concentration field tracks each one of the fluids, identifying the diffuse interface between them. A common correlation between viscosity and concentration is given by (Oliveira and Meiburg, 2011, 2017; John *et al.*, 2013; Heussler *et al.*, 2014; Oliveira and Meiburg, 2013; Tan and Homsy, 1988; Goyal and Meiburg, 2005; Yortsos and Zeibek, 1988; Manickam and Homsy, 1995; Islam and Azaiez, 2007; Chen and Meiburg, 2017):

$$\mu(c) = \mu_1 e^{\eta c}. \tag{5}$$

In equation Eq. (5), η is one of the dimensionless control parameters of our problem and represents the logarithmic-scale viscosity ratio, where μ_1 is the dynamic viscosity of the injected fluid, and μ_2 is the viscosity of the displaced fluid:

$$\eta = \ln\left(\frac{\mu_2}{\mu_1}\right). \tag{6}$$

The remaining dimensionless parameters that control the flow are the Reynolds number Re and the Galilei number or gravitational factor, F, and the Péclet number,

$$Re = \frac{\rho_1 U R_{ext}}{\mu_1}, \quad F = \frac{\Delta\rho g R_{ext}^2}{\mu_1 U}, \quad Pe = \frac{U R_{ext}}{D} \tag{7}$$

The Reynolds number (Re) relates inertial and viscous forces; the gravitational parameter (F) determines the influence of buoyancy between a pair of fluids with different densities; and the Péclet number characterizes mass transfer. Here, D is the diffusion coefficient of the transported substance, and ρ is a function that linearly correlates the constant density of each fluid.

3. NUMERICAL SOLUTION

The present work solves the axisymmetric Navier-Stokes equation with variable viscosity in cylindrical coordinates coupled with an advection and diffusion equation for a scalar field that describes the miscible displacement of a Newtonian fluid by injection of a second one in the annular region between two concentric pipes, where the outer pipe contains an abrupt expansion. We obtain flow velocities and concentrations of the displaced fluid to calculate efficiency of the miscible displacement. Thus, the work focuses on miscibility and its effects on the displacement process.

The discretization of equations was performed using finite differences combining the Adams-Bashforth, Runge-Kutta, and Crank-Nicolson techniques for temporal discretizations. For spatial discretization, central methods are used for diffusive terms and a fifth-order upwind technique for nonlinear terms. The calculation of the pressure field is done using the projection method and solved by spectral methods (Oliveira and Meiburg, 2011; Rai and Moin, 1991; Oliveira and Meiburg, 2017; John *et al.*, 2013; Heussler *et al.*, 2014; Oliveira and Meiburg, 2013). Graphical visualization is produced through MATLAB.

4. RESULT AND DISCUSSIONS

Since we are interested in the influence of miscibility on annular displacement flows, we focused on the influence of the Péclet number (Pe), keeping the remaining parameters fixed. They are Reynolds number, $Re = 1$; Log-viscosity ratio, $\eta = 2$, and $F = 0$, so the fluids are neutrally buoyant.

4.1 Convergence Analysis

A numerical convergence study was conducted to evaluate the mesh density. The original code utilizes a uniform square mesh with a resolution of 80 points per unit length. For a rectangular 10x1 domain, the chosen resolution employs 800x80 points. To verify that this resolution is suited for the current axisymmetric simulations, two essential hydrodynamic parameters were studied: fluid concentration c and axial displacement velocity v_z. The following strategy was employed to conduct this study:

1. Analysis of numerical meshes with resolutions N_zxN_r = 100x10, 400x40, 800x80, and 1500x150, where N_z defines the number of cells for the axial coordinate z, while N_r establishes the number of cells for the radial coordinate r;

2. Calculation of numerical errors of the axial velocity and concentration fields inside the expanded region at $t = 3.6$, a time when the interface is located in the washout.

Figure 2 shows the results of a simulation using these mesh resolutions. The simulation was conducted with the following dimensionless parameters kept fixed, $Re = 1$, $Pe = 1000$, $\eta = 2$, and $F = 0$, and $\Delta t = 1 \times 10^{-4}$. Through a preliminary qualitative analysis of Fig. 2, it can be observed that, although the 100x10 mesh is very coarse, it captures the interface location and its overall shape but misses quantitative precision. The remaining concentration contours are nearly indistinguishable from one another. Figure 3 calculates the numerical error with respect to the finer, 1500×150, mesh of averaged values of the concentration and axial velocity fields in the region for the contours located within $3.5 \leq z \leq 6.5$. We observe that the square mesh which employs 80 points per unit length in both directions exhibits a low percentage error, so it will be used throughout the study.

4.2 Displacement Efficiency

As discussed earlier, the relationship between variable viscosity and concentration field, as expressed in Eqs. (5) and (6), tracks each of the fluids and identifies the diffuse interface between them. Thus, average concentration values can be used to accurately calculate displacement efficiency. For example, at the initial condition, the geometry is mostly filled with the displaced fluid $Fluid$ 2, and the initial overall average concentration is close to $\overline{\overline{c}} = 1$. As the displacement progresses, the injected fluid $Fluid$ 1 begins to fill the domain, resulting in a gradual decrease in the average concentration. If the injected fluid $Fluid$ 1 displaces the resident fluid completely from the annulus, then we will find an overall average concentration value close to zero, $\overline{\overline{c}} = 0$. Therefore, displacement efficiency can be defined as $\epsilon = 1 - \overline{\overline{c}}$, where average of the concentration field is calculated considering the entire domain and both r and z directions.

It is important to highlight that, due to the diffuse nature of the interface and the presence of the concentration field that captures mass transport at the interface, this definition of efficiency is extremely interesting and well-suited for miscible displacements. Moreover, it contrasts with the typical approach based on the ratio between the area/volume occupied by the injected fluid employed when immiscible displacements are considered, cf. Naccache *et al.* (2018), Zhang *et al.* (2022), Shahriar and Nehdi (2012), McLean *et al.* (1967).

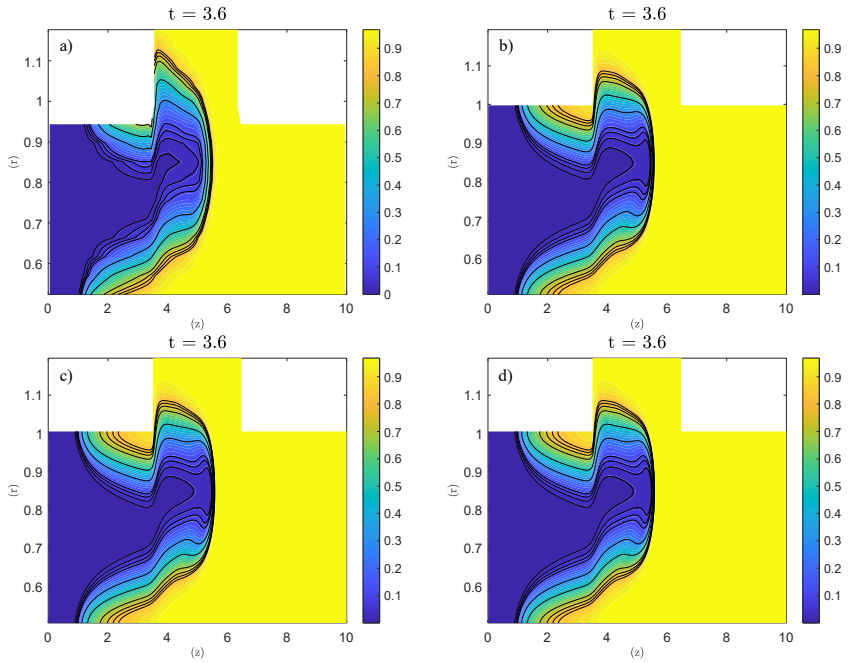

Figure 2. Simulated concentration front profiles for different numerical mesh densities at $t = 3.6$: a) 100x10 mesh, b) 400x40 mesh, c) 800x80 mesh, and d) 1500x150 mesh. The dimensionless parameters used were: $Re = 1$, $Pe = 1000$, $\eta = 2$, and $F = 0$.

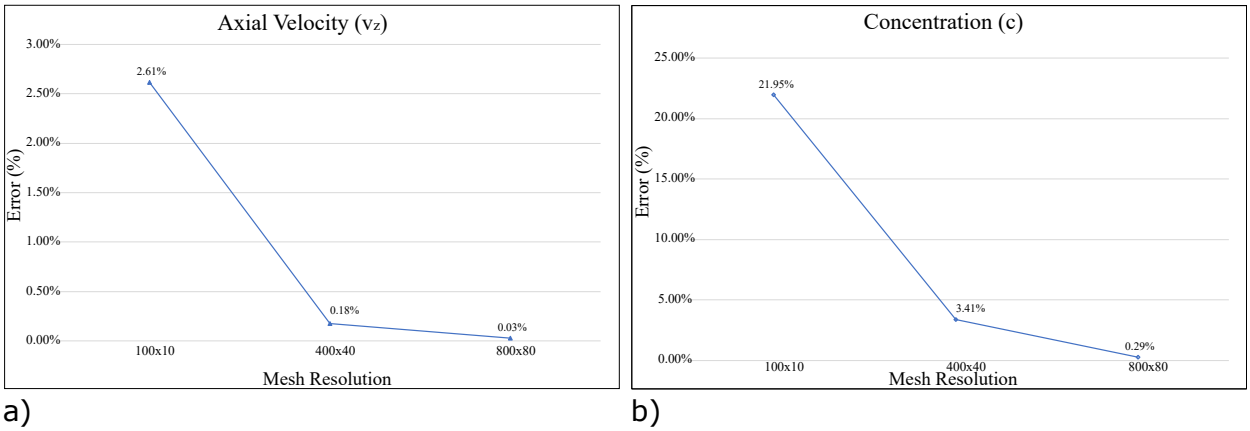

Figure 3. Curves of percentage errors in the expanded region for $3.5 \leq z \leq 6.5$ as a function of mesh density. a) Percentage error of axial velocity curves, and b) Percentage error of concentration profiles.

4.3 Effects of Miscibility

We analyze the displacement between two miscible fluids in an annular space that contains an abrupt expansion-contraction. The interfacial tension between the fluids is zero (Kuang *et al.*, 2004), and the interface is defined by a concentration gradient determined by the interplay between mass advection and diffusion. The Péclet number (Pe) is the dimensionless parameter used to quantify the relationship between these two modes of transport. So, it is the key parameter to capture the influence of miscibility at the interface between injected and displaced fluids, having fundamental importance for the analysis of the hydrodynamic behavior of the displacement flow.

To investigate the influence of miscibility, we vary the Péclet number across a wide range, as specified below. The chosen values have been related to diffusivity as reported in Savery *et al.* (2007).

- $Pe = 1000 \quad \longmapsto \quad D = 9.83 \times 10^{-5}\, pol^2/s$
- $Pe = 6000 \quad \longmapsto \quad D = 1.64 \times 10^{-5}\, pol^2/s$

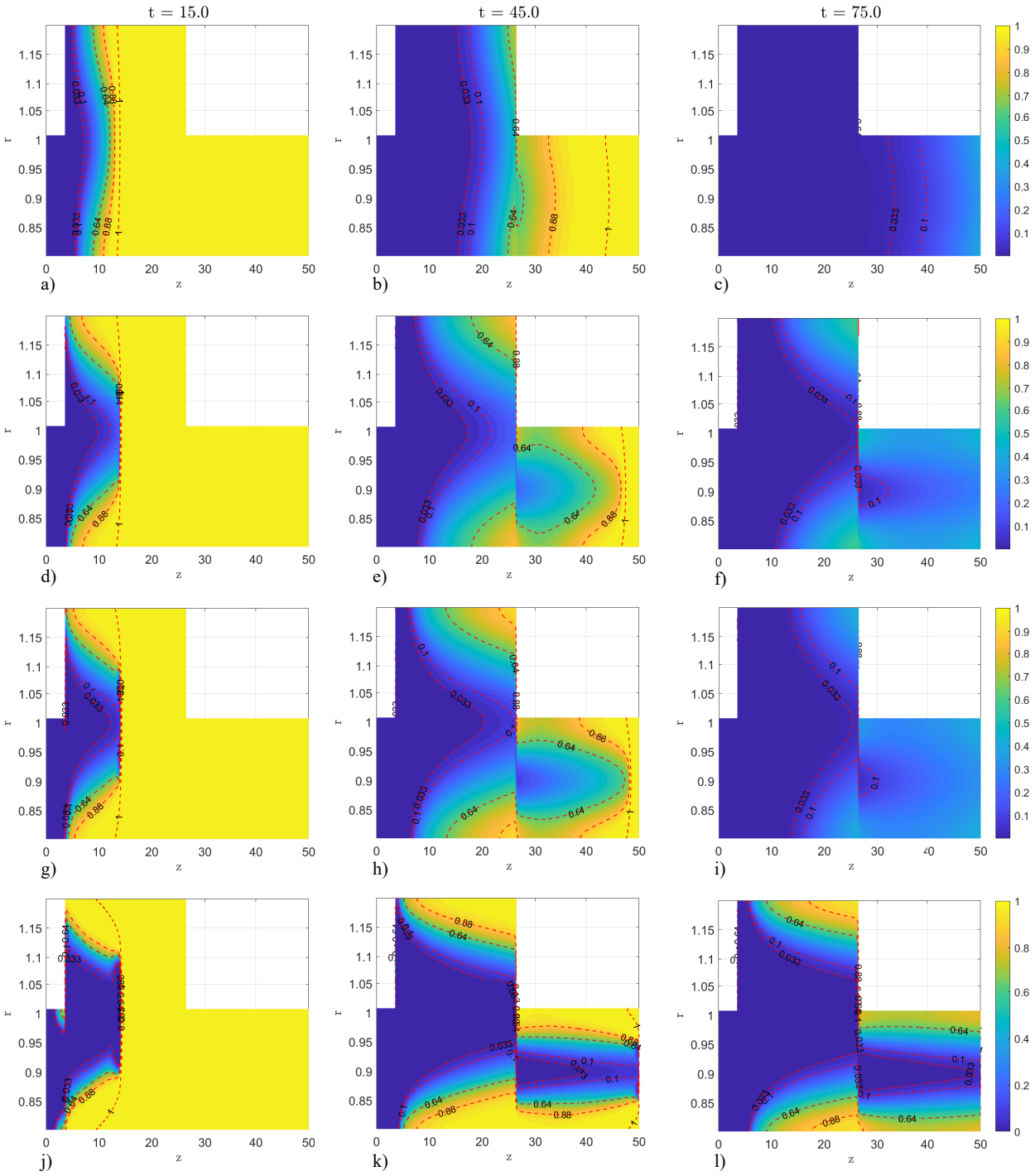

Figure 4. Simulations of different concentration propagation profiles with different Pe numbers (from top to bottom: 1000, 6000, 10000, and 50000), at non-dimensional times (from right to left: $t = 15$, $t = 45$, and $t = 75$). The expanded region measures 0.2 in thickness and is located in the interval $3.5 \leq z \leq 26.5$.

- $Pe = 10000 \qquad \longmapsto \qquad D = 9.38 \times 10^{-6}\, pol^2/s$
- $Pe = 50000 \qquad \longmapsto \qquad D = 1.97 \times 10^{-6}\, pol^2/s$

The remaining fixed parameters used in the following analysis are:

$$Re = 1, \qquad \eta = 2, \qquad F = 0 \tag{8}$$

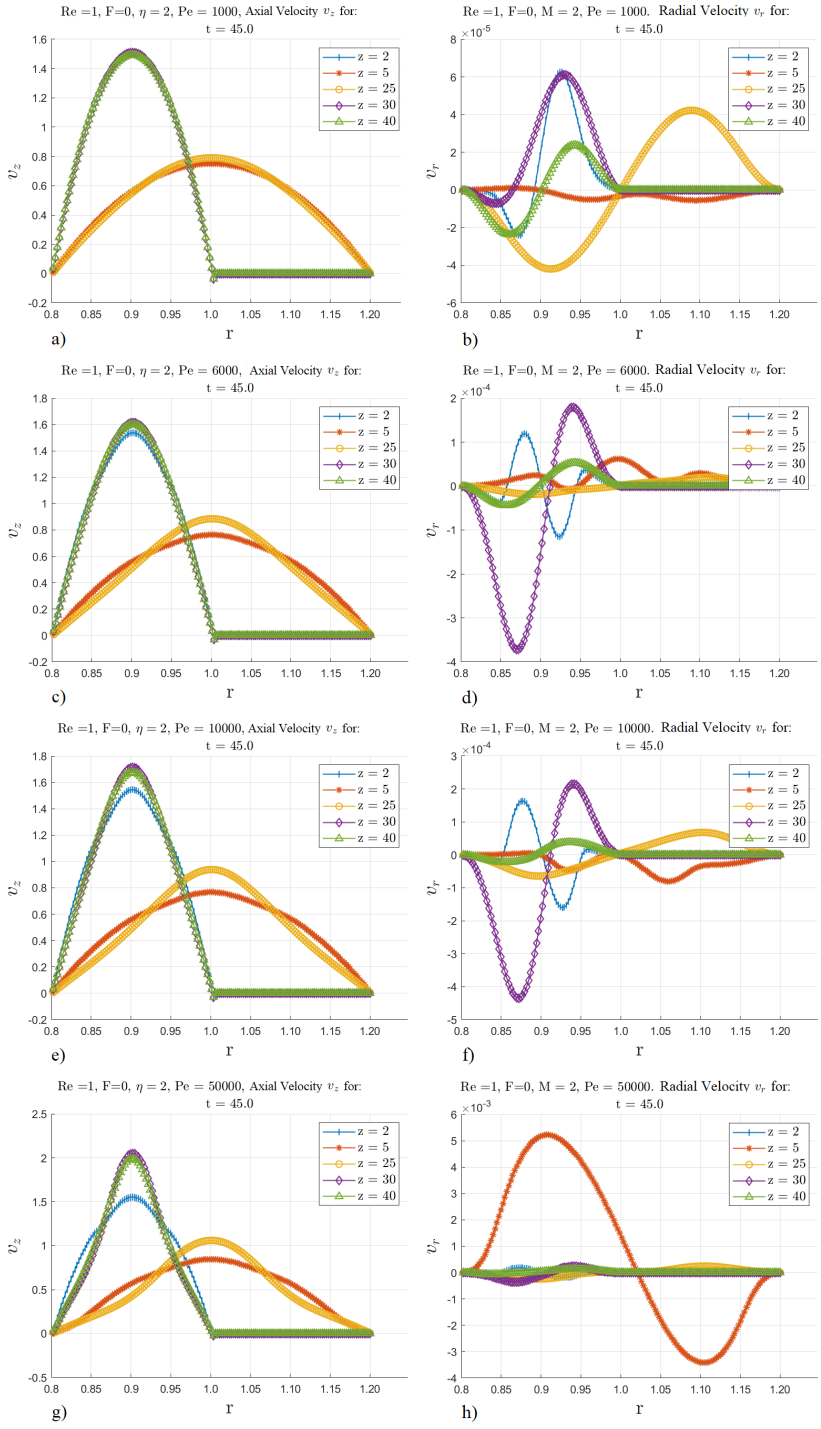

Figure 5. Profiles of axial velocities v_z on the left column, and radial velocities v_r on the right for different Péclet numbers, $Pe = 1000$, 6000, 10000, and 50000 at time instant $t = 45$. The color code indicates different positions along the axial axis, $z = 2$, 5, 25, 30, and 40.

We begin our discussion by looking at Figure 4. It shows concentration contours identifying the injected fluid in blue, the more viscous displaced fluid in yellow, and the miscible interface in color gradients for four different values of the Péclet number at three different time steps. Images on the left column display time $t = 15$, when the displacement is passing through the expansion. By comparing different images on this column for increasing Pe-values, we find sharper, better-defined interfaces indicating weaker diffusion for larger values of this parameter. One noteworthy feature is seen for the lowest value, $Pe = 1000$. It exhibits high diffusion, and the interface pattern is smoother, presenting a large mixed

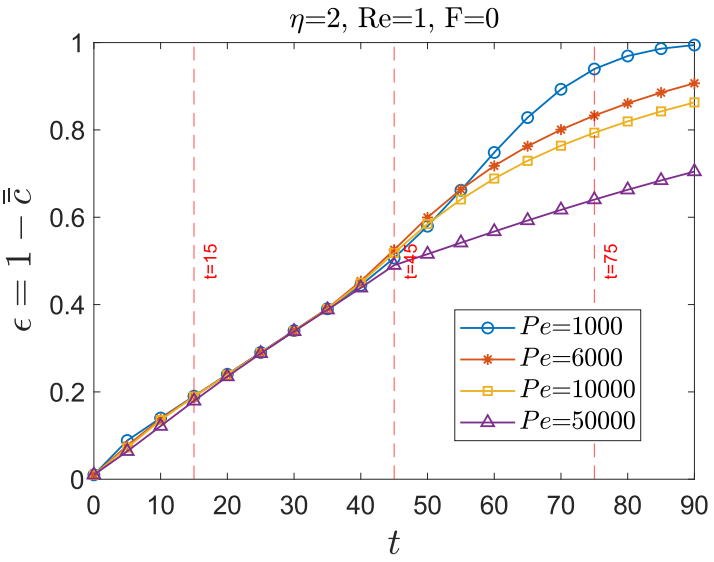

Figure 6. Displacement efficiency ϵ, calculated from the average concentration with respect to the radial and axial axes (r and z respectively) for various Péclet numbers, $Pe = 1000$, 6000, 10000, and 50000 in the time range $0 \leq t \leq 90$. As expected from the analysis of Fig. 4, the presence of high diffusion (lower Pe) at the fluid interface favors the achievement of high displacement efficiencies.

green area compared to the bottom case in which $Pe = 50000$. This has important implications for the displacement pattern. The radial concentration gradients for $Pe = 1000$ are reduced, and the interface length in the axial direction is smaller, meaning that smaller mixing lengths are found for stronger diffusive effects. As a consequence, the displacement process approaches the ideal one given by a plug. Notice that as time advances and we analyze the entire first row for $Pe = 1000$, the interface retains small deformations across the annular gap. In addition, as diffusion effects increase with time, the color gradient also becomes wider, cf. top frame in the middle column for $t = 45$. This behavior suggests that the resident fluid can be completely removed from the domain by the continuous inflow of the less viscous miscible fluid. We highlight that the influence of diffusion is fundamental in this process and we can expect to achieve very high values of displacement efficiency.

Another point observed is that in this study, we used an injected $Fluid$ 1 that is approximately 7.3 times less viscous than the displaced $Fluid$ 2, i.e. $\eta = 2$. The less viscous injected fluid has larger mobility. This favors penetration into the displaced fluid and the formation of increased mixing lengths. Here, the strong influence of interface diffusion for $Pe = 1000$ appears to counteract this tendency, and the mixing length is reduced.

In addition, due to a stronger diffusion at lower Péclet numbers (e.g., 1000), the injected fluid takes less time to mix and fills the spaces occupied by the displaced fluid. This is why it exhibits a less tapered concentration front and approaches a plug shape compared to the other cases with higher Péclet numbers, $Pe = 6000$, 10000, and 50000, where diffusion is slower. In contrast, the cases with large Pe values generate more elongated and tapered hydrodynamic profiles or bottleneck shapes.

Figure 5 provides important information regarding the relationship between the axial velocity v_z (left column) and radial velocity v_r (right column) for increasing values of the Péclet number (different rows). The color code indicates the velocity at different axial positions for a fixed time, $t = 45$. It can be observed that the maximum velocity of the axial v_z component undergoes significant growth with increasing Péclet numbers, regardless of its position on the axial axis. Physically, the narrowing of the concentration propagation profiles by a reduced diffusion as the Péclet number increases is caused by the reduced mixing capacity between the fluids. So less energy is dissipated by diffusion and a larger kinetic energy is maintained. This translates into the higher observed axial velocities closer to the center of the concentration profiles. Notice that a similar trend is also observed for the radial velocity, v_r, seen on the right column of Fig. 5. The magnitude of the vertical axis increases from 10^{-5} to 10^{-3} as Pe varies between $Pe = 1000$ and $Pe = 50000$. In addition, this quantity captures the washout-induced radial movement of the displacement front.

It is interesting to note that the flow undergoes acceleration after passing through the contraction. This can be observed by comparing the axial velocities v_z at positions $z = 2$, $z = 30$, and $z = 40$ (located before or after the contraction) with $z = 5$ and $z = 25$, located inside the expanded erosion. This is easily explained by mass conservation and is directly associated with changes in the cross-sectional area of the annular space.

Finally, we analyze Figure 6, which shows the displacement efficiency calculated by the average of the concentration

field, $\epsilon = 1 - \bar{\bar{c}}$. The efficiencies remain practically identical until time $t = 45$. From this moment on, the flows determined by higher Péclet numbers (6000, 10000, and 50000) show a reduction in displacement efficiency compared to the flow with $Pe = 1000$. The efficiencies values measured at the final simulated time, $t = 90$, are close to 100%, 90%, 76%, and 70%, respectively, for Péclet numbers $Pe = 1000$, 6000, 10000, and 50000. This is strong evidence that increased miscibility contributes to attaining high efficiencies. In addition, this motivates further studies and the analysis of the influence of diffusion considering different Reynolds numbers, and different fluid properties in displacements with both Newtonian and non-Newtonian fluids.

4.4 Conclusions and Future Works

The dissertation highlights the influence of diffusive processes in the displacement between miscible Newtonian fluids confined in an annular geometry containing a rectangular irregularity (washout). Using a DNS simulator, the numerical algorithm solves the Navier-Stokes equations with variable viscosity in cylindrical coordinates coupled with an advection-diffusion equation for the concentration field. This scalar variable tracks each fluid phase and identifies the diffusive interface between them.

For neutrally buoyant flows, fixed values of the viscosity ratio, and a fixed injection rate, we calculated interfacial displacement patterns for different values of the Péclet number (Pe) and analyzed the influence of diffusion on interface propagation velocity and displacement efficiency. Displacements with the highest diffusion investigated, $Pe = 1000$, smooth out the shearing concentration profiles, reducing their radial gradients. This hinders the formation of a thin film of the resident fluid during the displacement process. This phenomenon, when it occurs, appears to dominate the dynamics and favors the achievement of high displacement efficiencies.

This work emphasizes the importance of fluid miscibility in achieving high displacement efficiencies. A natural extension involves the comparison of these results to the limit in which diffusion is absent, $Pe- > \infty$. In addition, we also need to investigate how displacement efficiency is influenced by different values of the following controlling parameters: injection flow rates (Re), logarithmic viscosity ratios (η), Galilei numbers (F), and size of the washout. An important extension of this work should also consider the influence of miscibility in displacements involving non-Newtonian fluids.

5. ACKNOWLEDGEMENTS

This study was financed in part by the Coordenação de Aperfeiçoamento de Pessoal de Nível Superior - Brasil (CAPES) - Financing Code 001.

6. REFERENCES

Bittleston, S.H., Ferguson, J. and Frigaard, I.A., 2022. "Mud removal and cement placement during primary cementing of an oil well - laminar non-newtonian displacements in an eccentric annular hele-shaw cell." *Journal of Engineering Mathematics*, Vol. 43, pp. 229–253.

Chen, C.Y. and Meiburg, E., 2017. "Miscible displacements in capillary tubes. part 2. numerical simulations." *Phys. Rev. Lett.*, Vol. 118(12), p. 124502.

Etrati, A., Roustaei, A. and Frigaard, I.A., 2020. "Strategies for mud-removal from washouts during cementing of vertical surface casing". *Journal of Petroleum Science and Engineering*, Vol. 195.

Goyal, N. and Meiburg, E., 2005. "Miscible displacements in hele-shaw cells : two-dimensional base states and their linear stability". *J. Fluid Mech.*, Vol. 558, pp. 329–355.

Heussler, F.H.C., Oliveira, R.M., John, M.O. and Meiburg, E., 2014. "Three-dimensional navier-stokes simulations of buoyant, vertical miscible hele-shaw displacements". *J. Fluid Mech.*, Vol. 752, pp. 157–183.

Islam, M.N. and Azaiez, J., 2007. "New viscous fingering mechanisms at high viscosity ratio and péclet number miscible displacements." *J. Porous Media*, Vol. 10(4).

John, M.O., Oliveira, R.M., Heussler, F.H.C. and Meiburg, E., 2013. "Variable density and viscosity, miscible displacements in horizontal hele-shaw cells. part 2. nonlinear simulations". *J. Fluid Mech.*, Vol. 271, pp. 295–323.

Kuang, J., Petitjeans, P. and Maxworthy, T., 2004. "Velocity fields and streamline patterns of miscible displacements in cylindrical tubes". *Experiments in Fluids*, Vol. 37, pp. 301–308.

Manickam, O. and Homsy, G.M., 1995. "Fingering instabilities in vertical miscible displacement flows in porous media." *J. Fluid Mech*, Vol. 288, pp. 75–102.

McLean, R.H., Manry, C.W. and Whitaker, W.W., 1967. "Displacement mechanics in primary cementing". *Journal of Petroleum Technology*, Vol. SPE1488, pp. 251–260.

Naccache, M.F., Pinto, H.A.M. and Abdu, A., 2018. "Flow displacement in eroded regions inside annular ducts". *Journal of the Brazilian Society of Mechanical Sciences and Engineering*, Vol. 40:420.

Nelson, E.B., 1990. *Well Cementing*. Elsevier, Amsterdam, 2nd edition.

Oliveira, R.M. and Meiburg, E., 2011. "Miscible displacements in hele-shaw dells: Three-dimensional navier-stokes

simulations". *J. Fluid Mech.*, Vol. 687, pp. 431–460.

Oliveira, R.M. and Meiburg, E., 2013. "Three-dimensional vorticity configurations in miscible hele-shaw displacements". *ELSEVIER B. V.*, pp. 203–212.

Oliveira, R.M. and Meiburg, E., 2017. "Saffman-taylor instability and the inner splitting mechanism". *Physical Review Letters*, Vol. PRL 118, 124502.

Rai, M.M. and Moin, P., 1991. "Direct simulations of turbulent flow using finite-difference schemes". *Journal of Computational Physics*, Vol. 96, pp. 15–53.

Renteria, A., Makeli, A., Frigaard, I., Lund, B., Taghipour, A. and Ytrehus, J.D., 2018. "Displacement efficiency for primary cementing of washouts sections in highly deviated wells". *OFFSHORE TECHNOLOGY CONFERENCE*, Vol. SPE-191989-MS.

Roustaei, A., Gosselin, A. and Frigaard, I.A., 2015a. "Residual drilling mud during conditioning of uneven boreholes in primary cementing. part 1 : Rheology and geometry effects in non-inertial flows". *Journal of Petroleum Science and Engineering*, Vol. 220, pp. 87–98.

Roustaei, A., Gosselin, A. and Frigaard, I.A., 2015b. "Residual drilling mud during conditioning of uneven boreholes in primary cementing. part 2 : Steady laminar inertial flows". *Journal of Petroleum Science and Engineering*, Vol. 226, pp. 1–15.

Savery, M., Darbe, R. and Chin, W., 2007. "Modelling fluid interfaces during cementing using a 3d mud displacement simulator". *OFFSHORE TECHNOLOGY CONFERENCE*, Vol. OTC185113.

Shahriar, A. and Nehdi, M., 2012. "Rheological properties of oil well cement slurries". *ICE - Institute of Civil Engineering*, Vol. 165, pp. 25–44.

Tan, C.T. and Homsy, G.M., 1988. "Simulation of nonlinear viscous fingering in miscible displacement." *Phys. Fluids*, Vol. 31(6), pp. 1330–1338.

Yortsos, Y.C. and Zeibek, M., 1988. "Dispersion driven instability in miscible displacement in porous media." *Phys. Fluids*, Vol. 31(12).

Zare, M., Roustaei, A. and Frigaard, I.A., 2017. "Buoyancy effects on micro-annulus formation: Density stable displacement of newtonian-bingham fluids". *Journal of Non-Newtonian Fluid Mechanics*, Vol. 247, pp. 22–40.

Zhang, Z., Huang, Z., Zhou, Y., Sheng, M. and Wu, B., 2022. "Characteristic of spiral displacement process in primary cementing of vertical well washout". *Society of Petroleum Engineers*, Vol. SPE212288.

7. RESPONSIBILITY NOTICE

The authors are solely responsible for the printed material included in this paper.